PHYSICAL REVIEW B **70**, 205426 (2004)

Adsorbed rare-gas layers on Au(111): Shift of the Shockley surface state studied with ultraviolet photoelectron spectroscopy and scanning tunneling spectroscopy

Thomas Andreev,* Ingo Barke, and Heinz Hövel†
University of Dortmund, Experimentelle Physik I, D-44221 Dortmund, Germany

(Received 20 April 2004; published 23 November 2004)

The energetic position of the Au(111) Shockley surface state is compared before and after adsorbing different rare gas monolayers (Ar, Kr, and Xe). We used ultraviolet photoelectron spectroscopy (UPS) and scanning tunneling spectroscopy (STS) in combination to get more complete information by using the advantages of both methods. For determining the energetic position and the effective mass of the surface state in UPS an analytic mathematical method is used, which takes the finite angular resolution of the analyzer into account. We performed STS scans for the pure Au(111) surface as well as covered with a monolayer Kr and Xe. For an accurate analysis it is possible to use an extended Kronig-Penney model to take into account the influence of the $23\times\sqrt{3}$ reconstruction. We found that the first monolayer of a rare gas induces shifts of around 50–150 meV increasing with the gas atomic number, whereas a second monolayer has only a small influence of about 3–18 meV. Using an image potential model it is possible to characterize these shifts qualitatively. For a semiquantitative analysis the phase accumulation model is applied. Within this model we can describe the experimental data roughly with a Coulomb potential changing in dependence of the electron affinity and the dielectric constant of the rare gas.

DOI: 10.1103/PhysRevB.70.205426 PACS number(s): 73.20.At, 79.60.Dp, 68.37.Ef

I. INTRODUCTION

Shockley surface states are two-dimensional systems which are formed by electron confinement due to the surface band gap of the bulk material and the vacuum barrier of the surface. They are of fundamental interest as model systems for a two-dimensional free electron gas. The properties energetic position E_0, effective mass m^*, and the lifetime were investigated thoroughly for different materials. Some discrepancies existed in earlier studies in particular for the comparison of ultraviolet photoelectron spectroscopy (UPS) and scanning tunneling spectroscopy (STS). New high-resolution experiments are in better agreement, cf., e.g., Refs. 1–4.

Due to its location at the sample surface the surface state can be influenced significantly by adsorbing various materials. Depending on the adsorbate the effect turns out qualitatively different. While some materials induce a shift,[5] chemisorbed atoms and molecules often completely quench the surface state.[6] Here we want to focus on the change of the properties E_0 and m^* after adsorption of different rare-gas layers.[7–9] These rare gases induce a shift towards higher energies, and the variation of the adsorbed gas offers a handle to investigate the underlying interactions in a systematic way. For the systems discussed here, the adsorbate layers can be described with simple models and they form incommensurate two-dimensional layers on Au(111), whereby the interaction with other substrates can be more complicated.[10–14] In particular for the reconstructing Au(111) surface it is advantageous to use UPS and STS in combination. It helps to identify possible discrepancies between different experiments, e.g., due to variations in the sample preparation and allows a view on the results in a more complete frame.

With STS it is possible to measure the influence of adsorbates on the local density of states (LDOS) at different positions of the reconstruction. In order to determine the energetic position and the lifetime of the surface state we consider the local variation of the surface potential induced by the $23\times\sqrt{3}$ reconstruction.[15,16]

Angle resolved UPS allows to measure the energetic dispersion of the surface state for monolayers (ML) and multilayers of rare gases on Au(111). We include the finite angular resolution of the analyzer with an analytic model. With this we get more accurate data for the energetic position and the effective mass of the surface state.

For the discussion of the experimental results we use the surface potential and the so-called phase accumulation model, which allows us to classify these shifts with the properties electron affinity EA and the dielectric constant ε of the rare gas. Using a surface potential, which was applied before for image states[17,18] we can classify the positions of the surface state qualitatively. It is also possible to explain the difference between an adsorbed rare gas monolayer and a multilayer of rare gas.

For more quantitative calculations we use the phase accumulation model which was applied before mainly for image states and quantum well states.[19–21] Within this model it is possible to describe the barrier potential with either a step or a Coulomb potential. From the comparison of the measured and calculated positions of the surface state we find that the relevant potential for the surface state is essentially influenced by the electron affinity and the dielectric constant of the rare gas.

II. EXPERIMENT

The experiments were performed using low-temperature scanning tunneling microscopy (STM) which is combined with UPS in a common ultrahigh vacuum (UHV) system.[22] It consists of two main chambers, a preparation chamber equipped with a high-resolution hemispherical electron energy analyzer for UPS and an analysis chamber containing the low-temperature STM.

The STS data, either dI/dV spectra measured with varying V at a single position or dI/dV maps measured for fixed V, were taken under open loop conditions by lock-in detection. The set point before switching off the feedback loop was between $V=-1$ V and $V=+1$ V and the tunneling current varied from $I=0.1$ nA to $I=0.3$ nA. For the single point spectroscopy data we used a modulation voltage of 7 $\mathrm{mV}_{\mathrm{rms}}$ and a frequency around 700 Hz. The lock-in time constant was set to 30 ms and the acquisition time was $\geqslant$80 ms to avoid time constant effects. All STM and STS data were measured at $T=5$ K.

Our hemispherical analyzer has a radius of 125 mm. As a photon source we use HeI light with the energy of 21.2 eV. We have achieved with this setup a resolution of 10 meV.[22] In the experiments presented here we chose slightly lower energy resolutions with higher counting rates. We used an angular acceptance of about ±1° and the data point distance is set to 5 meV. For the UPS measurement and the sample preparation the Au(111) samples were mounted on a manipulator, which can be cooled down below $T=10$ K, by means of a liquid helium flow cryostat. This manipulator allows transferring cold samples between the two chambers and into the STM. The angular accuracy of the manipulator is about 0.2° for the adjustable rotation around the manipulator axis. The fixed angle perpendicular to the axis is $0° \pm 0.3°$.

The Au(111) single-crystal sample was prepared by repeated cycles of ion sputtering (1 keV Ar^+ or Kr^+ ions) and heating up to 900 K for 1 or 2 h. We checked the cleanliness of the sample by measuring the UPS peak of the Au(111) surface state, which is very sensitive to contamination. An ultimate check is imaging the sample in the STM. See for example Fig. 6, which shows the excellent sample quality after rare gas adsorption. Some contamination occurs during the low-temperature UPS measurements. We checked that the resulting decrease of the surface-state intensity was not significant on the time scale of the photoemission experiment. Alternatively also samples with a Au(111) film on mica were used. These films were produced in a separate vacuum chamber following the procedure of Ref. 23 by evaporation of a 100 nm Au film on freshly cleaved mica at $T=360$ °C. After introducing the Au/mica samples into the UHV system the surface was cleaned with ion sputtering (20 min) and heating (600 K). While the mesoscopic surface structure and the crystalline orientation was better defined for the Au(111) single crystal, the terrace areas were larger on the Au/Mica samples (cf. Sec. V).

A controlled number of rare-gas monolayers were dosed onto the samples by controlling the partial pressure with a quadrupole mass spectrometer and a leak valve. The exact time, partial pressure, and temperature for adsorbing well-defined monolayers of rare gases were determined with UPS by monitoring the p signals of the corresponding rare gas. The energetic position of the measured p signals gives us information about the film thickness of the adsorbed monolayers. The nth atomic layer has a signal which is shifted to lower energies compared to the first layer.[24–27] We monitored the peak integral of a specific p signal as a function of time to get the adsorption time and temperature at a given partial pressure. One example for this procedure is shown in Fig. 1. We used a constant rare-gas pressure (around 6×10^{-8} mbar) in the preparation chamber. Then we linearly decreased the temperature. When the signal of the p peak emerges, the monitored monolayer begins to grow. At this point we held the temperature constant and stopped the time Δt until the signal of the monolayer has saturated. This shows that the monolayer is complete. Because we fixed the temperature just below the limit for monolayer growth, the second monolayer cannot be adsorbed [cf. the phase diagram for Ar and Kr on Ag(111) (Ref. 28)]. If the temperature is set to a lower value (not shown) the signal decreases again after the first monolayer is complete. This is an indication that the second monolayer begins to grow and the signal of the first monolayer is attenuated. After the production of the desired coverage the gas flux is stopped which puts the pressure back into the UHV regime and the temperature is reduced far below the adsorption temperature. Both changes take only a few seconds and therefore stabilize the rare gas film in its final configuration for the UPS and STM/STS measurements.

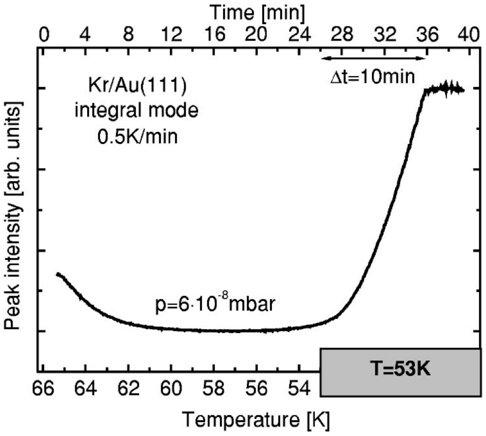

FIG. 1. Controlled adorption of the first ML Kr on Au(111) by monitoring the intensity integrated over the 4p peak. The temperature is ramped down from 66 K to 53 K with 0.5 K per minute and then held constant. The parameters time and temperature are indicated on the bottom and top scale, respectively. The signal decrease at the beginning of the measurement is caused by a drift of the channeltron counters after switching on their high-voltage supply.

This preparation method allows a perfect layer-by-layer growth which is shown in Fig. 2 for the adsorption of the first monolayer of Xe on Au(111). There the surface state peak of the clean Au(111) surface attenuates with increasing Xe coverage. Simultaneously a second peak appears at a higher energetic position. It corresponds to the shifted surface state on Xe/Au(111) and reaches maximum intensity at a coverage of one monolayer. STM images show that in the submonolayer regime the adsorbed Xe arranges in islands of several 1000 nm^2 [cf. also the STM images for Kr/Au(111) shown in Fig. 6]. Hence the energetic position does not shift continuously but the two systems Au(111) and Xe/Au(111) coexist in one sample.

III. UPS RESULTS

In the last decades angle resolved photoelectron spectroscopy has become an important tool for the observation of the

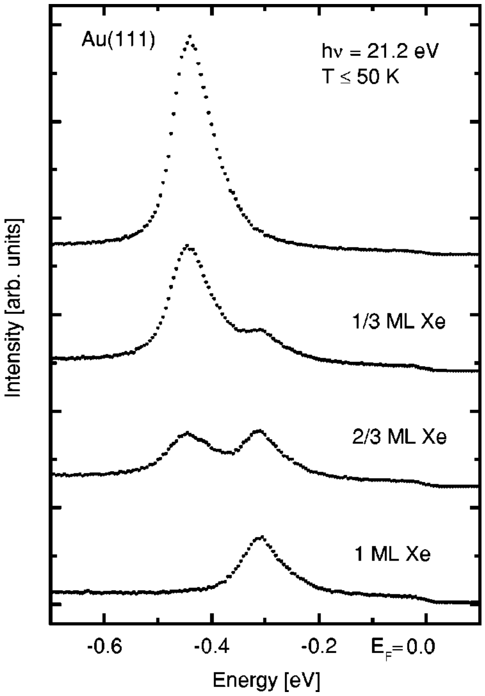

FIG. 2. UPS surface-state signal in normal emission of clean Au(111) and with increasing coverages of Xe.

surface state of metals. For the correct interpretation of the experiments it is important to consider the finite energetic and angular resolution of the electron analyzer. This problem is described extensively in Refs. 29 and 30.

Here we give an analytical mathematical expression for the influence of the finite angular resolution on a photoelectron spectra of an electron state with parabolic dispersion.

The energy dispersion of the surface state can be written as,

$$E = E_0 + \hbar^2 k_\parallel^2 / 2m^* \tag{1}$$

with the onset of the parabolic surface state E_0, and its effective mass m^*. The wave vector parallel to the surface is $k_\parallel = \sqrt{2mE_{Kin}/\hbar^2} \sin\theta$, E_{Kin} is the kinetic energy of the photoelectrons after leaving the surface, m is the free electron mass, and θ the angle of electron emission. In UPS only the parallel part of the k vector can be measured directly. The finite angular resolution of the electron analyzer applies not only for the angle α, which we are able to change by rotating the manipulator, but also for the angle β corresponding to the direction perpendicular to the manipulator axis, which is in our experiment adjusted at zero. We suppose that the distribution of the angles is Gaussian, because the aperture of the analyzer is small. A two-dimensional Gaussian function [Eq. (2)] gives the distribution around the adjusted angles α_0 and β_0:

$$P(\alpha,\beta) = \frac{1}{2\pi\sigma_\alpha^2} \exp\left[-\frac{(\alpha-\alpha_0)^2 + (\beta-\beta_0)^2}{2\sigma_\alpha^2}\right]. \tag{2}$$

In this formula σ_α is the angular resolution of the analyzer, which is assumed to be isotropic ($\sigma_\alpha = \sigma_\beta$).

For a realistic comparison between theory and experiment all angles have to be considered. The probability distribution of Eq. (2) can be transformed into an energetic one:

$$P(\alpha,\beta)d\alpha d\beta = P(E)dE.$$

Because for the surface state both angles α_0 and β_0 are small and $\sigma_\alpha \ll 1$, it is $\theta^2 = \alpha^2 + \beta^2 \ll 1$ and the energy (1) can be approximated as

$$E \approx E_0 + c\theta^2 \quad \text{with} \quad c = E_{kin}(m/m^*). \tag{3}$$

The use of cylinder coordinates ($\alpha = \theta\cos\varphi$ and $\beta = \theta\sin\varphi$) gives

$$P(E)dE = d\theta\theta \int_0^{2\pi} d\varphi P(\theta,\varphi)$$

with

$$P(\theta,\varphi) = \frac{1}{2\pi\sigma_\alpha^2} \exp\left[-\frac{(\theta\cos\varphi - \alpha_0)^2 + (\theta\sin\varphi - \beta_0)^2}{2\sigma_\alpha^2}\right].$$

Now we get for $P(E)dE$,

$$P(E)dE = d\theta\theta \frac{1}{2\pi\sigma_\alpha^2} \exp\left(-\frac{\theta^2 + \alpha_0^2 + \beta_0^2}{2\sigma_\alpha^2}\right) \times \int_0^{2\pi} \exp\left(\frac{2\theta\alpha_0\cos\varphi + 2\theta\beta_0\sin\varphi}{2\sigma_\alpha^2}\right) d\varphi. \tag{4}$$

Solving the integral in Eq. (4) leads to[31]

$$P(E)dE = d\theta\theta \frac{1}{\sigma_\alpha^2} \exp\left(-\frac{\theta^2 + \alpha_0^2 + \beta_0^2}{2\sigma_\alpha^2}\right) I_0\left(\frac{\theta}{\sigma_\alpha^2}\sqrt{\alpha_0^2 + \beta_0^2}\right).$$

In this formula I_0 is the regular modified cylindrical Bessel function of the order zero. After the substitution of $\theta = \sqrt{(E - E_0)/c}$ from formula (3) and $E_{kin}(E) = E + h\nu - \Phi$, where Φ is the work function, the probability distribution finally transforms to

$$P(E) = \frac{1}{2c\sigma_\alpha^2} \frac{E_{kin}(E_0)}{E_{kin}(E)} \exp\left[-\left(\frac{E - E_0}{c} + \alpha_0^2 + \beta_0^2\right)/2\sigma_\alpha^2\right] \times I_0\left(\sqrt{\frac{E - E_0}{c}} \frac{\sqrt{\alpha_0^2 + \beta_0^2}}{\sigma_\alpha^2}\right). \tag{5}$$

The function (5) has to be convoluted numerically with a Lorentzian (finite lifetime). As only occupied states contribute to the spectra, the result is multiplied with a Fermi function corresponding to the sample temperature T. Finally a convolution with a Gaussian is performed due to the finite energy resolution of the analyzer.

To fit the calculated set of spectra to the experiments we varied the following parameters: The energetic position E_0, the effective electron mass m^* of the surface state, the start angle α_{start} from where the others follow in the same distance (here 1°), the angular resolution σ_α, the width of the Lorentzian Γ, and the energy resolution σ_{Gauss}.

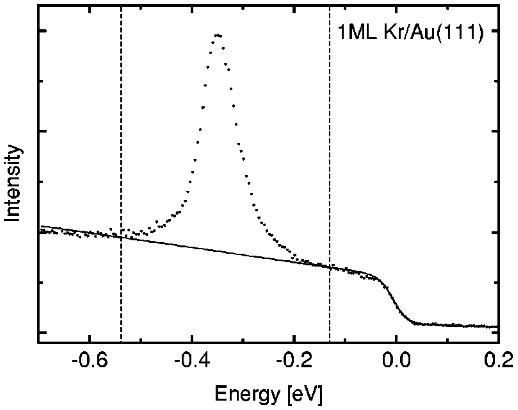

FIG. 3. The dots are the measured photoemission data for the angle nearest to zero. The line shows the calculated fit of a Fermi function multiplied with a linear function. The region between the dashed vertical lines was excluded for the fit.

To compare the measured data of the surface state to the calculated, we first have to subtract a background intensity. The background can be induced, for example, by satellites from the photon source or by signal from defects and it is approximated by a linear function. The structure of the background is angle independent for small angles. So we use the zero degree angle to fit a Fermi function multiplied with a linear function in a region without signal from the surface state. This is shown for one example in Fig. 3. With this fit we get the position of the Fermi energy E_F very accurately as well, which is needed to calculate the absolute energetic position of the surface state.

Angle resolved UPS spectra for a monolayer and a bilayer krypton on Au(111) are presented in Fig. 4, spectra for other rare gases in Fig. 5. For each sample system just one set of parameters as described above is used to fit all spectra for different angles simultaneously. Only a constant factor is adjusted for each curve individually to match the peak amplitudes. Generally the agreement between the calculated curves and the experiment is very good.

For the krypton bilayer in Fig. 4(b) the signal on the lower energy shoulder is higher than the calculated curve. This could be caused by photon induced desorption of a part of the second monolayer induced by the helium lamp, which leads to a small signal of the first monolayer krypton. A similar effect is also visible for Ar/Au(111) [cf. Fig. 5(d)].

It has to be taken into account that the mean free path of the electrons is finite in the rare-gas layers.[32] The surface state signal was around three to four times higher for the first monolayer krypton than for the second monolayer krypton. For this reason a higher accumulation time is needed for the second monolayer Kr.

The fit parameters σ_α $(0.7° - 1.1°)$, σ_{Gauss} (17 meV−45 meV), and Γ (18 meV−40 meV) used in Figs. 4 and 5 are not independent. Partly they are influenced by measurement artifacts as, e.g., errors for the adjustment of the angles α_0 and β_0 due to not perfectly flat sample surfaces, in particular for the Au/Mica samples. The angle β_0 was adjusted to 0° within ±0.3° at the sample holder. For the comparison with the experiment we also have to adjust the difference between the calculated starting angle α_{start} and zero which could be ±0.5°. The parameters E_0 and m^* for the different samples will be summarized in Sec. V.

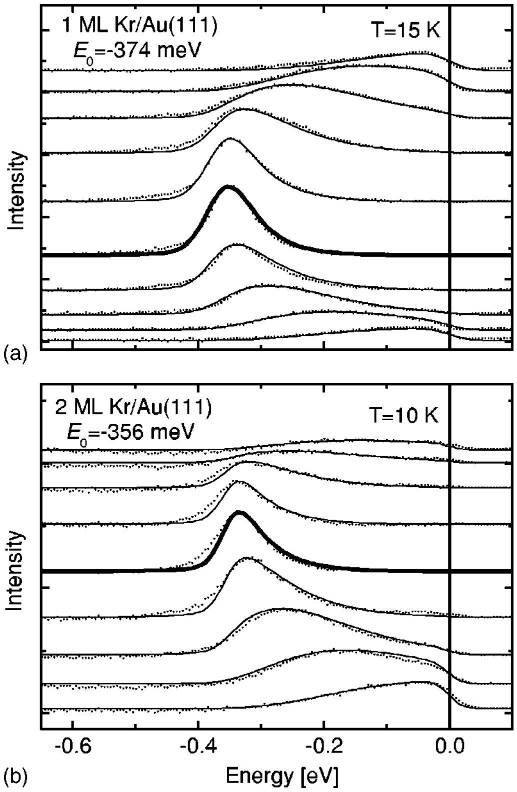

FIG. 4. High-resolution angle resolved photoemission curves of the surface state from Au(111) on mica covered with (a) one and (b) two monolayers krypton. The dots are the measured photoemission data after background subtraction and the solid lines show the calculated spectra from the model as presented here. The curves were measured in steps of 1.0°. Accumulation time per point: 1 s for the monolayer Kr, 2 s for the bilayer. A vertical line marks the position of the Fermi energy $E_F=0$. The calculated spectrum closest to normal emission is plotted with a thick line.

With the fitting routine we were much more sensitive for calculating the energetic position and the effective electron mass for the dispersion relation of the surface state than by simply measuring peak positions. For example, the lowest peak position in Fig. 4(a) would indicate $E_0 \approx -347$ meV which is 27 meV too high, mainly because of the systematic error induced by the asymmetric broadening due to the finite angular resolution.

IV. STS RESULTS

With STS we are able to measure the energetic position of the surface state onset very accurately. It is possible to change the position of the tip and measure in different regions of the reconstruction and far away from step edges and defects.

The periodic Au(111) reconstruction $(a=6.3\text{ nm})$ can be separated into a fcc, a hcp, and two transition regions.[33–36] Figure 6 shows two STM images, one overview picture which shows the clean Au(111) surface and parts covered

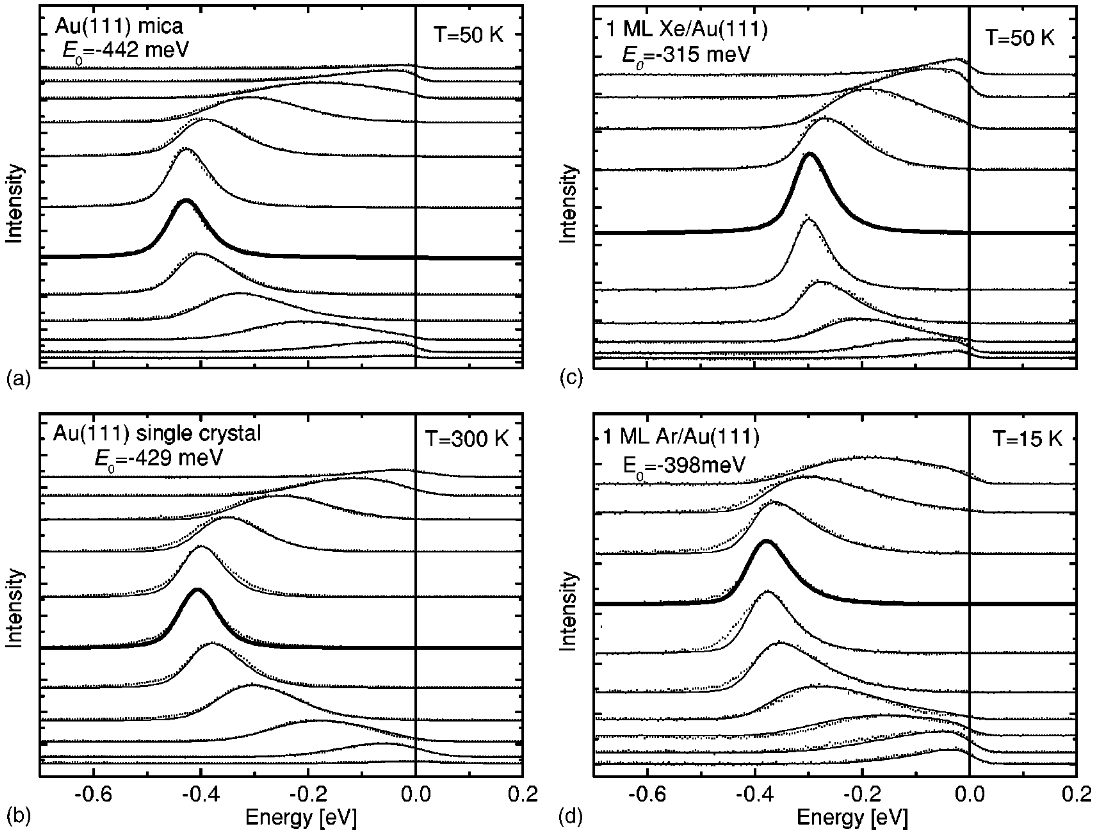

FIG. 5. High-resolution angle resolved photoemission curves of the surface state from (a) Au(111) on mica at $T=50$ K and (b) Au(111) single crystal at room temperature. The spectra for Au(111) on mica covered with (c) Xe and (d) Ar were measured at $T=50$ K or 15 K, respectively. The dots are the spectra for each angle with the background subtracted and the solid line shows the calculated spectra. A vertical line marks the position of the Fermi energy $E_F=0$. The calculated spectrum closest to normal emission is plotted with a thick line.

with 1 ML krypton [Fig. 6(a)], and an atomically resolved image of the Au(111) reconstruction with one monolayer krypton adsorbed [Fig. 6(b)]. The few bright dots on the uncovered Au(111) terraces in Fig. 6(a) correspond to small Kr islands located at the step edges but partly also at the knees of the herringbone reconstruction. White horizontal lines indicate that some of these islands are shifted by the tip. The dark spots on the rare gas covered part are vacancies in the Kr film. Some of them occur as horizontal lines also indicating a tip surface interaction. The $23\times\sqrt{3}$ reconstruction is visible on both, the clean and the Kr covered, areas. The bright dots in Fig. 6(b) represent the atomic structure of the krypton layer, which is incommensurate to the Au(111) surface. The two bright stripes are the transition regions and the part inside is the hcp region. Outside the transition region, the fcc region is imaged as the broader part.

The influence of the reconstruction on the surface state was considered in Ref. 15 by applying a Kronig-Penney model for the periodic effective potential with the width a_1 in the fcc regions and a_2 in the hcp regions:

$$V_{KP}(x)=\begin{cases} V_1 & \text{for } 0\leqslant x<a_1 \\ V_2 & \text{for } a_1\leqslant x<a_1+a_2 \end{cases} \quad ; \quad V_{KP}(x+a_1+a_2)=V_{KP}(x).$$

A special lock-in technique for mapping the surface potential spacially resolved was used in Ref. 16. A strongly structured potential was found at the transition regions of the reconstruction in addition to the difference between hcp and fcc sites. We obtained a similar result by observing that the Kronig-Penney potential as used in Ref. 15 could not reproduce all features in the experimental STS spectra. The agreement was significantly better if we extended the Kronig-Penney model with δ distributions at the narrow transition regions. The extended Kronig-Penney potential $V_{EKP}(x)$ can be summarized as

$$V_{EKP}(x)=V_{KP}(x)+V_{\delta}(x) \text{ with } V_{\delta}(x)=A[\delta(x)+\delta(x-a_1)].$$

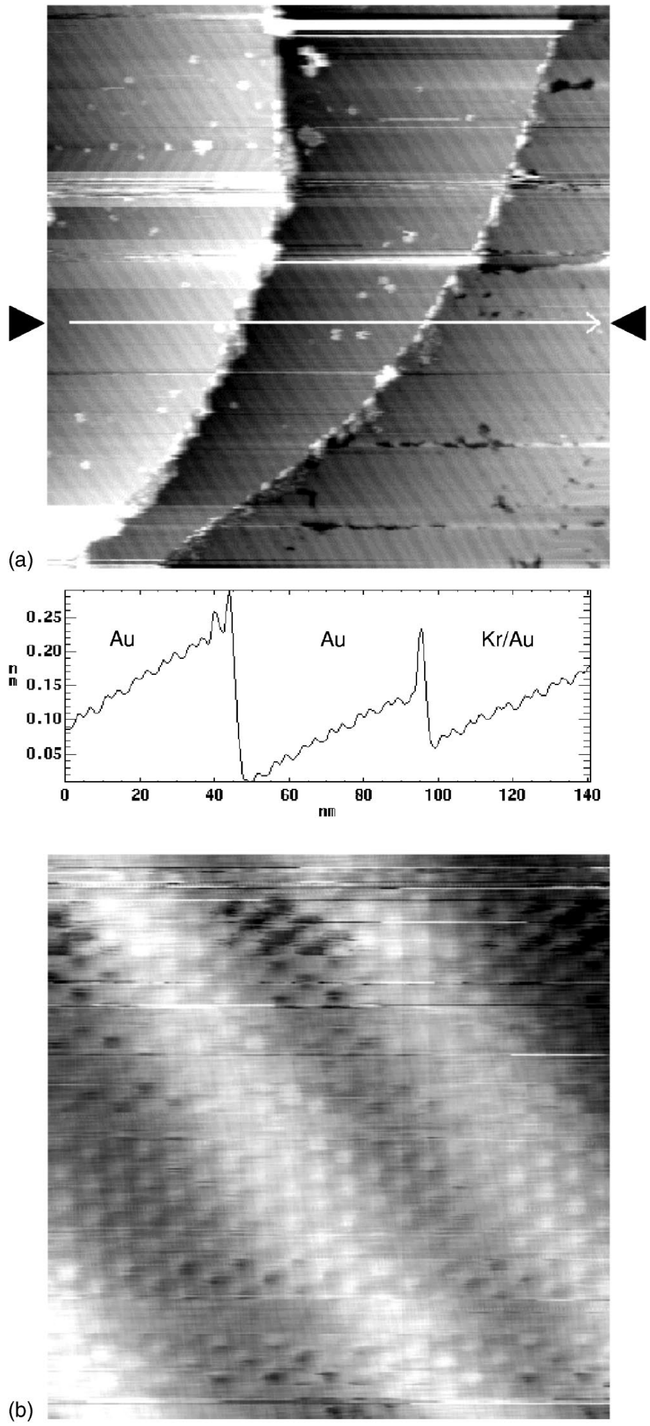

FIG. 6. (a) Top: STM image ($150\times150\ \mathrm{nm}^2$) of Au(111) on mica partly covered with Kr; bottom: line profile marked in the top image (b) STM image ($7\times7\ \mathrm{nm}^2$) of one stripe of the reconstruction of Au(111) on mica covered with a monolayer krypton (sample voltage −0.93 V, tunneling current 0.24 nA).

The intensity A of the δ distribution can be either negative or positive. The potential also satisfies the periodicity condition:

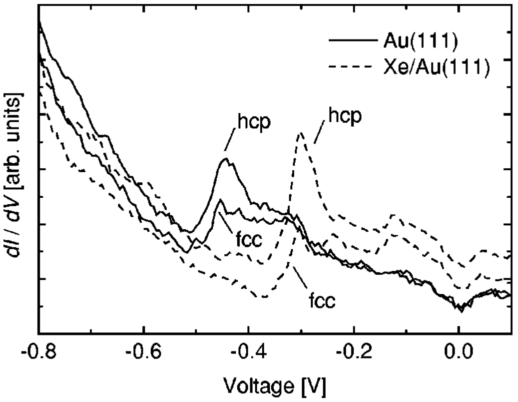

FIG. 7. Measured dI/dV spectra for a clean Au(111) surface (solid) and a Xe covered Au(111) surface (dashed). Each spectrum is an average of 25 single spectra which enhances the signal/noise ratio. For both systems the spectra were taken in the center of the hcp region as well as in the fcc region.

$$V_{EKP}(x+a_1+a_2)=V_{EKP}(x).$$

Here we compare the measured STS data with the calculated density of states of the extended Kronig-Penney model. The two-dimensional local density of states LDOS (E,x,y) can be written as

$$\mathrm{LDOS}(E,x,y)=\frac{V}{2\pi^2}\frac{d}{dE}\int_{\varepsilon(k_x,k_y)\leqslant E}|\psi_{k_x,k_y}(x,y)|^2dk_x\,dk_y,$$

where $\varepsilon(k_x,k_y)$ is the electron dispersion relation. To consider the one-dimensional influence of the reconstruction we have to split the wave function in a free-electron like y component and a Bloch component in x direction:

$$\psi_{k_x,k_y}(x)\propto e^{ik_yy}e^{ik_xx}u_{k_x}(x).$$

Here $u_{k_x}(x)$ is a function with the periodicity of the reconstruction. From this we get for the LDOS (E,x),

$$\mathrm{LDOS}(E,x)\propto\int_{\varepsilon(k_x)\leqslant E}\frac{|\psi_{k_x,k_y}(x,y)|^2}{\sqrt{E-\varepsilon(k_x)}}dk_x.$$

With the potential $V(x)$ we have the complete Hamiltonian and we are able to calculate the wave function within the transfer matrix formalism.[37] The density of states is evaluated numerically. The calculation can be compared with the STS spectra after a convolution with a Gaussian and a Lorentzian function.

For Au(111) and Xe/Au(111), respectively, measured raw data are shown in Fig. 7. The measured STS spectra show the step-shaped onset of the surface state at $V\approx-0.5$ V and $V\approx-0.35$ V, respectively, superimposed on a background which is given by the transmission coefficient.[38] Using

TABLE I. Energetic position of the surface state for different rare-gas systems on Au(111) measured with STS and UPS. The effective electron mass was determined from the UPS fit described above. For 2 ML Xe/Au(111) only the normal emission spectrum was taken. For some systems we show values for different samples. Some complement values for Cu(111) and Ag(111) are given in Ref. 7–9.

System	Energetic position UPS (meV)	Energetic position STS (meV)	Effective mass m^*/m_e
Au(111) single crystal	−429 (T=300 K) and −487 T=30 K from Ref. 49	−499 to −494	0.26 and 0.255 from Ref. 49
1 ML Xe/Au(111) single crystal	⋯	−349 and −363	⋯
Au(111) Mica	−442 and −453	−465 and −469	0.245 and 0.23
1 ML Ar/Au(111) Mica	−400	⋯	0.24
1 ML Kr/Au(111) Mica	−374	−414	0.27
2 ML Kr/Au(111) Mica	−356	⋯	0.28
1 ML Xe/Au(111) Mica	−315	−319	0.25
2 ML Xe/Au(111) Mica	−312	⋯	⋯

$$T(d,V) \propto \exp\left\{-2d\sqrt{\frac{2m_e}{\hbar^2}\left(\overline{\phi}-\frac{eV}{2}\right)}\right\}$$

with the tip surface distance d and the mean work function $\overline{\phi}$, the background signal can be fitted to the low-voltage tail of the spectra, assuming a constant bulk density of states. In addition one observes peaks and kinks which display characteristic differences for measurements in the hcp and fcc region.

For the calculated data we adjusted four free parameters: a_1, $\Delta V = V_1 - V_2$, and A, which determine the shape of the spectra, and the absolute energetic position V_1. We used an effective electron mass of $m^* = 0.24 m_e$, which is the average value measured for the Au(111) surface state with UPS (see Sec. V). A possible change of m^* by the rare gas is negligible for this calculation (cf. Table I). For a clean surface the lifetime of the Au(111) surface state is between $\tau = 31$ fs (Ref. 3) and $\tau = 35$ fs.[2] For the system Xe/Ag(111) a lifetime decrease of the surface state was observed.[9] For Au(111) we could neglect this effect and use the same Lorentzian line width of 18 meV for all coverages. This indicates that the lifetime change is not strong compared to the lifetime of the clean surface. The width of the Gaussian is $\sigma = 5$ meV, which is the energy resolution of our experimental setup.[39] We notice here that the observed agreement in the width of the step onset and the first peak in the hcp region (cf. Fig. 8) corroborates the lifetimes of Refs. 2 and 3. The sum $a = a_1 + a_2 = 6.3$ nm is the period length of the reconstruction.[33–36] From different STM pictures no significant change of the reconstruction was found after adsorbing different rare gases, in contrast to the significant change of reconstruction after adsorbing oxygen.[40]

Figure 8 shows STS data for a single Au(111) crystal and Kr on Au(111) on mica after subtraction of the background signals as discussed in the context of Fig. 7. The experimental spectra are compared with the calculated LDOS. The overall shape of this spectrum roughly corresponds to the step function expected for the two-dimensional density of states. In the hcp region of the reconstruction we see in addition a peak at the step onset, which is caused by the one-dimensional influence of the reconstruction. In the fcc region the surface state onset exhibits a reduced LDOS. The essential structures are reproduced by the model, i.e., the first peak in the hcp region at the surface state onset, as well as the feature at the second band gap of $E(k_\parallel)$ at $V \approx -350$ mV for clean Au(111), respectively, $V \approx -270$ mV for Kr/Au(111). The main parameter for the amplitude of the peak in the hcp region is ΔV and it changes from 18–39 meV for pure Au(111), to 50 meV for Kr/Au(111), and from 65–70 meV for Xe/Au(111). This indicates that also the local modulation of the potential is modified by the rare-gas layer.

Without adding the δ distributions to the Kronig-Penney model, we could only find agreement between calculated and measured LDOS with extremely asymmetric ratios a_1/a_2, in particular concerning the feature at the second band gap. This would be contradictory to experimental measured reconstruction widths.[41,33]

Here we focus on the spatially averaged potential which can be calculated as

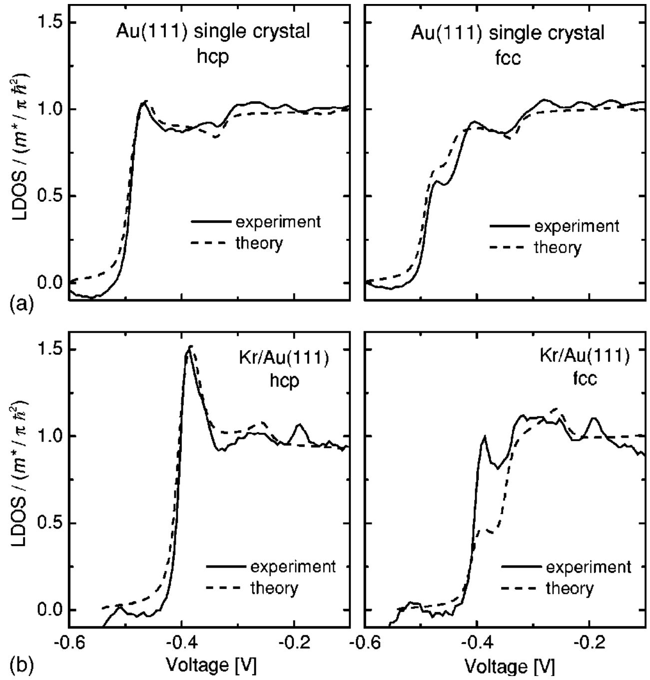

FIG. 8. STS spectrum of the surface state (a) of a clean single crystal and the (b) for Kr/Au(111) on mica, in the hcp (left) and the fcc (right) region, respectively. The calculated LDOS curves are plotted with dashed lines and the experimental dI/dV spectra are normalized to the calculated curves. We used a_1=3.15 nm, ΔV =18 meV, $\langle V\rangle$=−494 meV, and A=−22 meV nm for Au(111) and a_1=3.15 nm, ΔV=50 meV, $\langle V\rangle$=−414 meV, and A=+35 meV nm for Kr/Au(111), respectively. Because the different fit parameters have independent effects on the calculated LDOS, it is possible to arrive at unique parameter sets by manually fitting the experimental curves.

$$\langle V\rangle = \frac{a_1V_1 + a_2V_2 + 2A}{a_1 + a_2}.$$

Hence by considering the extended Kronig-Penney model we are able to calculate the energetic position of the surface state more accurately. The value of $\langle V\rangle$ which is given by the STS measurement far away from step edges and defects can be compared to the energetic positions observed with UPS, which averages over a macroscopic area.

V. DISCUSSION

One influence for the energetic shift of the surface state induced by the rare gas, may be the change of the work function. We determined the work function for, e.g., clean Au(111) to 5.36 eV and Xe/Au(111) to 5.04 eV by using the full energy width of the UPS spectrum, i.e., the difference between the Fermi energy E_F and the low energy onset of the secondary electrons E_{SE}, as $\phi = h\nu - (E_F - E_{SE})$. For these work function spectra a sample bais of −5 V was applied. Considering only the work function change a small shift of the surface state to lower energies would be expected[19] but we get an upward shift of the surface state after rare-gas adsorption, in opposite direction to the work function change. So other effects have to be considered.

UPS averages over a macroscopic area of the sample (in our measurements an area of about 3 mm diameter), and therefore includes defect induced signals. The data from STS are measured on large plane areas of the surface. So by combining both methods we can estimate the possible influences from step edges and other defects, which induce a shift to higher energies,[42,43] an asymmetry of the surface state peak in UPS (Ref. 44), and local variations in the density of states.[45,46]

In Table I the measured energetic positions of the surface state for different rare-gas systems are given. The comparison between the measured UPS and STS data shows the effect of spatial averaging in UPS. The energetic position of the surface state is always lower in STS, which is consistent with the arguments before. In addition the influence of the tip-surface potential[47] shifts the surface state as measured with STS about 15 meV to lower energies for the clean Au(111) surface.[48]

The surface state also shifts by using different types of Au(111) samples. With the STM we observed a larger number of small terraces for the single crystal used here than for Au(111) on mica. We think that this was caused by some residual stress of the crystal in the sample holder, because we observed distorted shapes for the herringbone reconstruction. On the other hand, there are cloughs between the different Au crystallites on mica. Inside these cloughs no surface state exists. The small single crystallites for Au(111) on mica may be mechanically stressed too. Stress affects the shape of the reconstruction[35] and causes a shift of the surface state.[50] From four series of data we get the position of the surface state of the Au(111) single crystal between −494 meV and −499 meV in STS. On Au(111) on mica we have measured a position of the surface state around 30 meV higher: between −465 meV and −469 meV (see Table I).

In addition it has to be noticed that the Au(111) on mica sample is not as plane as the single crystal. So the angular distribution can be broader in UPS.

For an exact comparison we have to consider the different temperatures of the measurements.[51] Higher temperatures induce a shift of the surface state of about 0.2 meV/K to higher energies. This is most important for the UPS data of the Au(111) single crystal [Fig. 5(b)], which were measured at room temperature. For the comparison of the STS and the UPS data at temperatures from 5 K to 50 K this effect is small because it is induced by a changing of the lattice parameters which levels off at low temperatures. We observed no significant change of the effective electron mass m^* (cf. Table I) after adsorption of different rare gas monolayers, in agreement with results for rare gases on Ag(111) and Cu(111).[7–9]

Now we summarize and discuss the data for the several different rare-gas systems measured in this work. In the UPS data of Table I and Fig. 9 we can see that the shift of the surface state is small after adsorbing a second monolayer, whereas different rare gases induce significantly different shifts. The corresponding STS data for the clean and 1 ML systems are systematically shifted to lower energies due to the local character of the measurement[44–46] and the influence of the tip-surface potential[47,48] as discussed above. But the

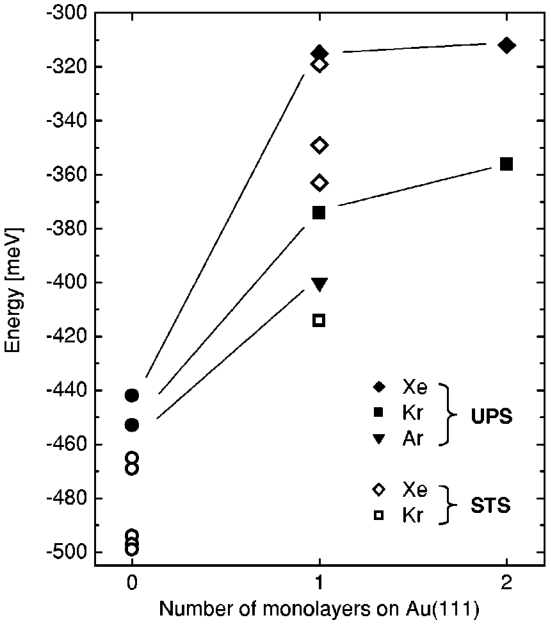

FIG. 9. Energetic position of the surface state of Au(111) after adsorbing different rare gases (one and two monolayers). The number zero identifies the substrate itself. The symbol shape distinguishes between the different rare gases. UPS results are indicated by full symbols, whereas for the data points derived from STS measurements open symbols are used. The UPS data points for different rare gases are connected to guide the eye, whereby intermediate positions do not exist.

general effect of the rare-gas coverage is confirmed and the relative shifts are similar to the UPS data. We also note that the relative shifts for 1 ML Ar, Kr, and Xe as compared to the clean surface are in good agreement with UPS data for Cu(111).[7]

The potential change induced by the rare gas is investigated in Refs. 17 and 18. The rare-gas monolayer is described by a dielectric medium, positioned between the metal surface and the vacuum. The image potential in the vacuum and the rare-gas film can be calculated by the following functions:[17,18]

Inside the rare gas it is

$$V_i = -\frac{e^2}{16\pi\varepsilon_0\varepsilon z} + \frac{e^2(\varepsilon-1)}{16\pi\varepsilon_0\varepsilon(\varepsilon+1)(t-z)} + \frac{e^2(\varepsilon-1)(t+2z)}{16\pi\varepsilon_0\varepsilon(\varepsilon+1)(t+z)t} + \delta V_i(z) - \mathrm{EA}$$

with

$$\delta V_i(z) = -\frac{e^2 z^2}{8\pi\varepsilon_0\varepsilon t^3}\sum_{k=2}^{\infty}\frac{(-1)^k}{k(k^2 - z^2/t^2)}\left(\frac{\varepsilon-1}{\varepsilon+1}\right)^k. \qquad (6)$$

In the vacuum the potential is given by

$$V_a = -\frac{e^2}{8\pi\varepsilon_0(\varepsilon+1)z} - \frac{e^2(\varepsilon-1)}{16\pi\varepsilon_0(\varepsilon+1)(z-t)} + \delta V_a(z)$$

with

$$\delta V_a(z) = -\frac{e^2\varepsilon t}{4\pi\varepsilon_0(\varepsilon+1)^2 z}\sum_{k=1}^{\infty}\frac{(-1)^{k-1}k}{(kt+z)}\left(\frac{\varepsilon-1}{\varepsilon+1}\right)^k.$$

Here ε_0 is the vacuum dielectric constant, ε the dielectric constant of the rare gas film, t the thickness of the film, e the elementary charge, and EA the electron affinity of the rare gas (see below for EA values used). To overcome the singularity at $z=t$ the potential is interpolated linearly within a layer of 0.3 nm thickness.[17,18]

For ε we have used the bulk values given in the Refs. 52 and 53: $\varepsilon_{Ar}=1.56$, $\varepsilon_{Kr}=1.78$, and $\varepsilon_{Xe}=1.98$. Low-energy electron diffraction studies of rare gases on metals have shown that the lattice parameter of the first rare-gas monolayer can be different compared to the bulk.[54] This small influence is neglected in the following calculations.

Using this potential, we now qualitatively interpret the shifts induced by different rare gases and coverages. For a quantum well of the same width but with a higher barrier the electronic states shift to higher energies. If the width is getting narrower the states also shift but the relative effect is much stronger. In Fig. 10(a) we calculate the potential for different layer thicknesses of Xe. One can see that inside the quantum well, for energies around or below the Fermi energy E_F the width is the same for all rare-gas film thicknesses. Additional layers of Xe change the quantum well mainly at the top. So the influence on the surface state, with an energetic position some hundred meV below the Fermi energy, is small. If the rare gas is changed we get a small change at the top of the potential but the width changes at the bottom [Figs. 10(b) and 10(c)]. So we see that from Ar to Xe the potential is getting narrower and we can explain the large shift induced by using different rare gases, compared to the small shift of additional rare-gas monolayers.

In Fig. 10(c) it is visible that the width of the potential changes the most between the clean Au(111) surface and the different rare gases. This is in disagreement with the experiment, for which the relative shifts are of similar size going from the clean surface to Ar, Kr, and Xe. Possible reasons for this disagreement will be discussed later.

Quantitative values for the energetic positions of the surface state can be calculated using the phase accumulation model. The model consists of two reflection phases: the barrier phase and the crystal phase. If the sum of the barrier phase Φ_B and the crystal phase Φ_C is a multiple of 2π, i.e., $\Phi_B+\Phi_C=2\pi n$, bound states (so called image states) occur. For the special case of the surface state the sum $\Phi_B+\Phi_C$ must be zero.

This model is well suited to describe the position of the image states and the quantitative results are sensitively dependent on the exact position of the image plane z_0.[19,20,55]

The image state properties of different metal adsorbate interfaces were studied in the past (see e.g., Refs. 17, 18, 56, and 57). The model is described in detail in Refs. 19, 20, 57, and 58.

The crystal phase can be calculated as in Refs. 21 and 55 by

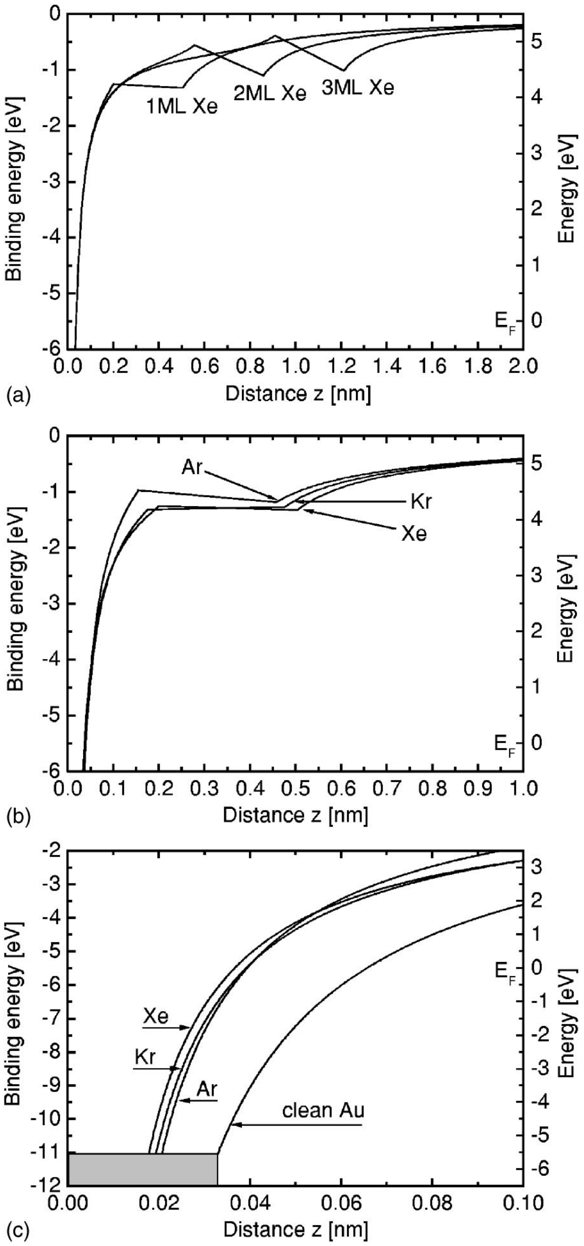

FIG. 10. Image potentials calculated using Eq. (6) for (a) one, two, and three monolayers Xe (b) one monolayer Ar, Kr, and Xe. The potential close to the surface is shown in (c). The potential is plotted regarding to the vacuum energy (binding energy) and the Fermi energy E_F, respectively. In (c) the gray box illustrates the position of the lower band edge for the conduction electrons, 5.51 eV below the Fermi energy, of a free electron gas with the parameters of gold (r_S=3.01 Bohr radii). The potential for a clean Au surface corresponding to Eq. (7) with $\varepsilon=1$ is added.

$$\Phi_C(E) = 2\arcsin\sqrt{\frac{E - E_L}{E_U - E_L}}.$$

In this equation $E_L=-1.05$ eV and $E_U=3.35$ eV are the positions of the lower and upper surface band gap of an Au(111) single crystal.[1]

The experimental results in Table I and Fig. 9 show that the influence of the second rare gas monolayer is small. Therefore it is useful to compare the energetic position of the surface state calculated for an infinite number of monolayers with the measured data of one and two monolayers rare gas.

Two possible potential models for the barrier phase are the step potential and the Coulomb potential. Both are interesting to consider because they, respectively, take into account different aspects of the rare-gas layer and the substrate.

The image potential of Eq. (6) changes for an infinite thickness of rare gas to a Coulomb potential considering the dielectric constant ε of the rare gas:

$$V = -\frac{e^2}{4\pi\varepsilon_0\varepsilon}\frac{1}{4z}. \tag{7}$$

For a clean metal surface ($\varepsilon=1$) the barrier phase for the Coulomb potential as given in Ref. 19 can be rationalized using the binding energies of the image states ($n=1,2,3,\ldots$) with respect to the vacuum energy E_V in the limit of an infinite barrier at the crystal surface ($\Phi_C=-\pi$) (Ref. 20):

$$E_n - E_V = -\frac{1}{16}E_{Ryd}\frac{1}{n^2}.$$

This gives for $\varepsilon=1$ (cf. Ref. 58)

$$\Phi_B^{Coul}(E) = \sqrt{\frac{E_{Ryd}/4}{E_V - E}} - \pi.$$

A dielectric constant $\varepsilon \neq 1$ changes the Rydberg energy

$$E_{Ryd}(\varepsilon) = \frac{m_e e^4}{32\pi^2\hbar^2(\varepsilon\varepsilon_0)^2} = \frac{13.6\text{ eV}}{\varepsilon^2}.$$

Together with the shift of the vacuum energy by the electron affinity EA of the rare gas this results in

$$\Phi_B^{Coul}(E,\varepsilon) = \sqrt{\frac{3.4\text{ eV}/\varepsilon^2}{E_V - \text{EA} - E}} - \pi.$$

We use for the vacuum energy E_V=5.3 eV (Ref. 1) and for the electron affinity $\text{EA}_{\text{Ar}}=-0.4$ eV, $\text{EA}_{\text{Kr}}=0.3$ eV and $\text{EA}_{\text{Xe}}=0.5$ eV, respectively.[52]

The reflection phase for the step potential is only influenced by the electron affinity:[19,20]

$$\Phi_B^{step}(E) = 2\arctan\left(-\sqrt{\frac{E_V - \text{EA}}{E - E_F}}\right).$$

For calculating the bound states we use the alternative crystal termination which fixes the image plane at the crystal surface and allows the electrons to propagate freely in a range of z_0.[19,20] This results in the following equation which defines the energetic position of the bound states with a free parameter z_0:

$$\Phi_B + \Phi_C + 2k_\perp z_0 = 0.$$

In the surface band gap $k_\perp \approx \pi/a$ (Ref. 21) will not change significantly for the small energetic shifts considered here. For the phase shifts given by $k_\perp z_0$ we assume a constant value for all samples, which is adjusted to the experimental position of the surface state for the Ar covered surface. The

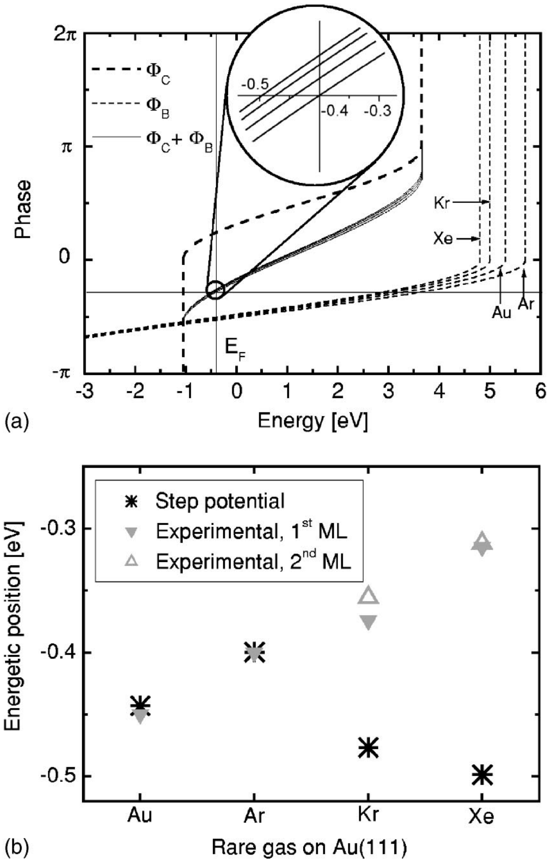

FIG. 11. (a) The crystal phase (fat dashed) and the barrier phase (thin dashed) and their sum (solid) are plotted for pure Au(111) and Ar, Kr, and Xe on Au(111) for a step barrier. The vertical and horizontal thin lines show the adjustment of the phase offset $k_{\perp}z_0$ for Ar/Au(111). In the inset the region determining the energetic position is magnified. (b) Energetic position of the surface state of clean Au(111) and after adsorbing different rare gases. The graph shows the experimental UPS values compared to the calculated ones for the step potential. For Kr and Xe both experimental values, for 1 ML and 2 ML, are given.

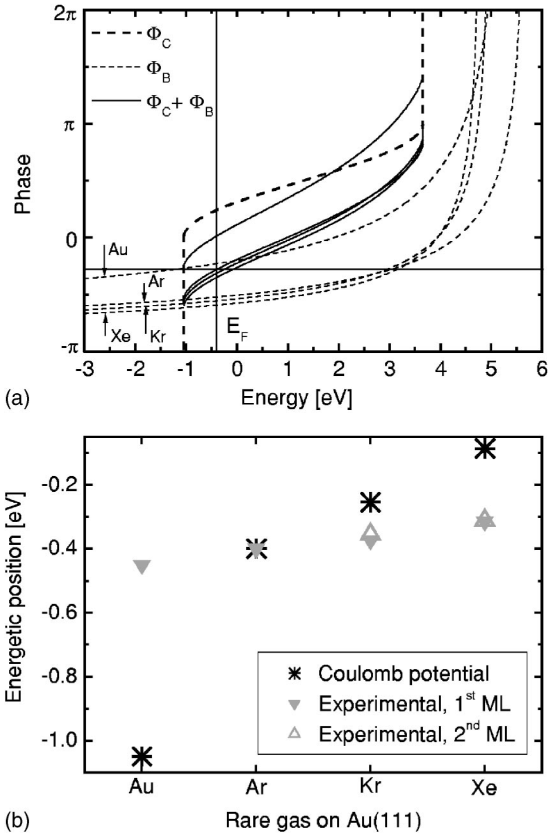

FIG. 12. (a) The crystal phase (fat dashed) and the barrier phase (thin dashed) and their sum (solid) are plotted for pure Au(111) and Ar, Kr, and Xe on Au(111) for a Coulomb potential. The vertical and horizontal thin lines show the adjustment of the phase offset $k_{\perp}z_0$ for Ar/Au(111). (b) Energetic position of the surface state of clean Au(111) and after adsorbing different rare gases. The graph shows the experimental UPS values compared to the calculated ones for the Coulomb potential. For Kr and Xe both experimental values, for 1 ML and 2 ML, are given.

reason for this choice will be discussed below.

First we discuss the energetic positions calculated with a step potential in Fig. 11.

In Fig. 11(b) it is visible that the calculated shifts disagree qualitatively with the experiment in case of Kr and Xe though the magnitude of the rare-gas induced shifts is of the order of 0.1 eV as in the experiment. The only influence considered here is the electron affinity EA of the rare gas. Its sign determines the main direction of the shift.

In Fig. 12(b) the calculated relative shifts for the different adsorbed rare gases using the Coulomb potential occur in the same qualitative direction as experimentally observed. It has to be noticed that the shift between the clean surface and the rare-gas covered surfaces is largely overestimated. This behavior can be explained as follows. It is visible in Fig. 12(a) for the Coulomb phase and in Fig. 10(c) for the image potential that the largest difference occurs between the rare-gas covered and the clean surface. This is in disagreement with the experiment. Possibly the large shift predicted with the Coulomb potential is partly compensated by a change of, e.g., the image plane z_0. In order to focus on the comparison between the different rare gases we fixed the image plane on the position of the surface state for Ar on Au(111).

The calculated relative shifts for the three different rare gases in Fig. 12(b) are of the correct magnitude but in absolute numbers about a factor of 3 larger than in the experiment. This discrepancy would be even worse for the bare Coulomb potential [cf. Eq. (7)] without changing the value of EA. The difference between Ar and Xe ($\varepsilon_{\mathrm{Ar}}=1.56$; $\varepsilon_{\mathrm{Xe}}=1.98$) would then be about as large as the difference between Ar and vacuum. The close "bunching" of the rare-gas potentials [cf. Fig. 10(c)] and barrier phases (cf. Fig. 12) only occurs due to the combination of the respective values of EA and ε which partly cancel in their effects.

For a quantitative comparison of calculation and experiment the exact values of ε for the different rare gases would be essential. However, a correction of the bulk parameters was needed, e.g., to explain the experimental results for studies of the image states.[59] For thin rare-gas films this may be connected to a lattice constant different to the bulk value.[54]

To summarize the discussion, we started from the experimental observation that the main shift of the surface state energy is already induced by the first ML of rare gas and we compared calculations for a half space of rare gas above the sample surface within the phase accumulation model using a step and a Coulomb potential. In this way we were able to distinguish between the general trends given by the macroscopic parameters EA and ε of the different rare gases. It is interesting to compare this to the interpretation of the surface state shift as due to the Pauli repulsion between the rare-gas atom and the metal,[60,61] for which also the interaction with the rare-gas atoms directly at the surface is crucial.

For a better determination of the surface state position a calculation is needed, which takes into account the potential near the surface on an atomic scale, as used for the surface- and image-state properties of clean Au(111) and Ag(111).[49,62] Of course these results have to be combined with the influence of the rare gas, as it was done for the case of image states for Ar/Cu(100).[56] But the main effects will be described already with semiquantitative model potentials as used here.

VI. CONCLUSION

On a Au(111) surface with a controlled number of adsorbed rare-gas monolayers we characterized the surface state with STS and UPS. The combination of both techniques helped to identify possible influences of, e.g., step edges and other defects and it presents a rather complete view of the effects induced by the rare-gas coverage.

For the angle resolved UPS data we included the finite angular resolution in a model which can be calculated analytically. For the STS data an extended Kronig-Penney model reproduced the structures induced by the influence of the $23\times\sqrt{3}$ reconstruction and helped us to quantify the surface-state onset. Calculating $\langle V\rangle$ from this model we can evaluate the spatially averaged energetic position of the surface state. The rare gas on Au(111) induces a shift of the surface state. We measured that the first monolayer of the different rare gases produces a shift between 50 to 150 meV and the second monolayer adds only a small additional shift of around 10 meV.

These shifts are interpreted qualitatively by an image potential, which was used for image and quantum well states before. Assuming that the dielectric constant and the electron affinity are the main characteristic parameters of the rare gas for the shift of the surface state, we can calculate the position of the surface state with a phase acculumation model. This model is applied to a rare-gas film of infinite thickness, because already the influence of the second monolayer was found to be small in the experiment. For the barrier phase we used different potentials. The step potential only includes the electron affinity of the rare gas, whereas the Coulomb potential additionally comprises the dielectric constant ε. The comparison with the measured surface-state positions reveals that a realistic phase has to take into account both, the dielectric constant and the electron affinity. However, for a quantitative theoretical determination of the rare-gas influence on the surface state the electronic interactions will have to be considered on an atomic scale using more advanced and therefore more complex techniques.

Note added in proof. It is interesting to compare the band-gap features in the STS spectra (cf. Fig. 8) with the density of states of the surface-state electrons on the reconstructed Au(111) surface as determined in Ref. 63 using angle-resolved photoemission.

ACKNOWLEDGMENTS

The authors would like to thank B. Grimm for important experimental contributions. This work was supported by the Deutsche Forschungsgemeinschaft (Grant Nos. Ho-1597/3-3 and SPP 1153).

---

*Present address: CEA/CNRS/UJF research group Nanophysique et Semiconducteurs, 17 rue des Martyrs, 38054-Grenoble cedex 9, France.

†Corresponding author; electronic address: hoevel@physik.uni-dortmund.de

[1] R. Paniago, R. Matzdorf, G. Meister, and A. Goldmann, Surf. Sci. **336**, 113 (1995).

[2] J. Kliewer, R. Berndt, E. V. Chulkov, V. M. Silkin, P. M. Echenique, and S. Crampin, Science **288**, 1399 (2000).

[3] F. Reinert, G. Nicolay, S. Schmidt, D. Ehm, and S. Hüfner, Phys. Rev. B **63**, 115415 (2001).

[4] O. Jeandupeux, L. Bürgi, A. Hirstein, H. Brune, and K. Kern, Phys. Rev. B **59**, 15 926 (1999).

[5] J. Repp, G. Meyer, and K.-H. Rieder, Phys. Rev. Lett. **92**, 036803 (2004).

[6] S. A. Lindgren and L. Wallden, Solid State Commun. **28**, 283 (1978).

[7] F. Forster, G. Nicolay, F. Reinert, D. Ehm, S. Schmidt, and S. Hüfner, Surf. Sci. **532**, 160 (2003).

[8] J. Y. Park, U. D. Ham, S. J. Kahng, Y. Kuk, K. Miyake, K. Hata, and H. Shigekawa, Phys. Rev. B **62**, R16 341 (2000).

[9] H. Hövel, B. Grimm, and B. Reihl, Surf. Sci. **477**, 43 (2001).

[10] J. F. Zhu, H. Ellmer, H. Malissa, T. Brandstetter, D. Semrad, and P. Zeppenfeld, Phys. Rev. B **68**, 045406 (2003).

[11] S. Clarke, G. Bihlmayer, and S. Blügel, Phys. Rev. B **63**, 085416 (2001).

[12] P. S. Bagus, V. Staemmler, and C. Wöll, Phys. Rev. Lett. **89**, 096104 (2002).

[13] B. Grimm, H. Hövel, M. Bödecker, K. Fieger, and B. Reihl, Surf. Sci. **454**, 618 (2000).

[14] B. Grimm, H. Hövel, M. Pollmann, and B. Reihl, Phys. Rev. Lett. **83**, 991 (1999).

[15] W. Chen, V. Madhavan, T. Jamneala, and M. F. Crommie, Phys. Rev. Lett. **80**, 1469 (1998).

[16] L. Bürgi, H. Brune, and K. Kern, Phys. Rev. Lett. **89**, 176801 (2002).

[17] J. D. McNeill, R. L. Lingle, R. E. Jordan, D. F. Padowitz, and C. B. Harris, J. Chem. Phys. **105**, 9 (1996).

[18] A. Hotzel, G. Moos, K. Ishioka, M. Wolf, and G. Ertl, Appl. Phys. B: Lasers Opt. **68**, 615 (1999).
[19] N. V. Smith, Phys. Rev. B **32**, 3549 (1985).
[20] N. V. Smith, Rep. Prog. Phys. **51**, 1227 (1988).
[21] M. Milun, P. Pervan, and D. P. Woodruff, Rep. Prog. Phys. **65**, 99 (2002).
[22] H. Hövel, T. Becker, D. Funnemann, B. Grimm, C. Quitmann, and B. Reihl, J. Electron Spectrosc. Relat. Phenom. **88–91**, 1015 (1998).
[23] M. Levin, A. Laakso, H. E.-M. Niemi, and P. Hautojärvi, Appl. Surf. Sci. **115**, 31 (1997).
[24] T. Mandel, G. Kaindl, M. Domke, W. Fischer, and W. D. Schneider, Phys. Rev. Lett. **55**, 1638 (1985).
[25] T. C. Chiang, G. Kaindl, and T. Mandel, Phys. Rev. B **33**, 695 (1986).
[26] K. Jacobi, Phys. Rev. B **38**, 5869 (1988).
[27] T. Mandel, M. Domke, and G. Kaindl, Surf. Sci. **197**, 81 (1988).
[28] J. Unguris, L. W. Bruch, E. R. Moog, and M. B. Webb, Surf. Sci. **109**, 522 (1981).
[29] R. Paniago, R. Matzdorf, G. Meister, and A. Goldmann, Surf. Sci. **331**, 1233 (1995).
[30] R. Matzdorf, Surf. Sci. Rep. **30**, 153 (1998).
[31] I. S. Gradshteyn and I. M. Ryzhik, *Tables of Integrals, Series und Products* (Academic Press, Orlando, 1980).
[32] T. Goulet, J. M. Jung, M. Michaud, J. P. Jay-Gerin, and L. Sanche, Phys. Rev. B **50**, 5101 (1994).
[33] Ch. Wöll, S. Chiang, R. J. Wilson, and P. H. Lippel, Phys. Rev. B **39**, 7988 (1989).
[34] J. V. Barth, H. Brune, G. Ertl, and R. J. Behm, Phys. Rev. B **42**, 9307 (1990).
[35] U. Tartaglino, E. Tosatti, D. Passerone, and F. Ercolessi, Phys. Rev. B **65**, 241406(R) (2002).
[36] H. Bulou and C. Goyhenex, Phys. Rev. B **65**, 045407 (2002).
[37] J. Schnakenberg, *Algorithmen in der Quantentheorie und Statistischen Physik* (Zimmermann-Neufang, Ulmen 1995).
[38] V. A. Ukraintsev, Phys. Rev. B **53**, 11 176(1996).
[39] H. Hövel, Appl. Phys. A: Mater. Sci. Process. **72**, 295 (2001).
[40] L. Huang, P. Zeppenfeld, J. Chevrier, and G. Comasa, Surf. Sci. **352**, 285 (1995).
[41] U. Harten, A. M. Lahee, J. P. Toennies, and Ch. Wöll, Phys. Rev. Lett. **54**, 2619 (1985).
[42] K. Morgenstern, K. F. Braun, and K. H. Rieder, Phys. Rev. Lett. **89**, 226801 (2002).
[43] A. Mugarza, A. Mascaraque, V. Repain, S. Rousset, K. N. Altmann, F. J. Himpsel, Yu. Koroteev, E. V. Chulkov, F. J. Garcia de Abajo, and J. E. Ortega, Phys. Rev. B **66**, 245419 (2002).
[44] A. Beckmann, K. Meinel, Ch. Ammer, M. Heiler, and H. Neddermeyer, Surf. Sci. **375**, L336 (1996).
[45] M. Pivetta, F. Silly, F. Patthey, J. P. Pelz, and W.-D. Schneider, Phys. Rev. B **67**, 193402 (2003).
[46] Y. Hasegawa and P. Avouris, Phys. Rev. Lett. **71**, 1071 (1993).
[47] L. Limot, T. Maroutian, P. Johansson, and R. Berndt, Phys. Rev. Lett. **91**, 196801 (2003).
[48] J. Kröger, L. Limot, H. Jensen, R. Berndt, P. Johansson, Phys. Rev. B **70**, 033401 (2004).
[49] G. Nicolay, F. Reinert, S. Hüfner, and P. Blaha, Phys. Rev. B **65**, 033407 (2001).
[50] G. Neuhold and K. Horn, Phys. Rev. Lett. **78**, 1327 (1997).
[51] R. Paniago, R. Matzdorf, G. Meister, and A. Goldmann, Surf. Sci. **336**, 113 (1995).
[52] M. L. Kein and J. A. Venables, *Rare Gas Solids II* (Academic Press, London, 1975).
[53] J. Marcoux, Can. J. Phys. **48**, 244 (1970).
[54] R. H. Roberts and J. Pritchard, Surf. Sci. **54**, 687 (1976).
[55] F. Patthey and W. D. Schneider, Phys. Rev. B **50**, 17 560 (1994).
[56] D. C. Marinica, C. Ramseyer, A. G. Borisov, D. Teillet-Billy, and J. P. Gauyacq, Surf. Sci. **528**, 78 (2003).
[57] C. Gahl, K. Ishioka, Q. Zhong, A. Hotzel, and M. Wolf, Faraday Discuss. **117**, 191 (2000).
[58] S. Hüfner, *Photoelectron Spectroscopy* (Springer, Berlin, 1995).
[59] W. Berthold, F. Rebentrost, P. Feulner, and U. Höfer, Appl. Phys. A: Mater. Sci. Process. **78**, 131 (2004).
[60] E. Bertel and N. Memmel, Appl. Phys. A: Mater. Sci. Process. **63**, 523 (1996).
[61] F. Reinert, J. Phys.: Condens. Matter **15**, S693 (2003).
[62] A. Garcia-Lekue, J. M. Pitarke, E. V. Chulkov, A. Liebsch, and P. M. Echenique, Phys. Rev. B **68**, 045103 (2003).
[63] F. Reinert and G. Nicolay, Appl. Phys. A: Mater. Sci. Process. **78**, 817 (2004).